

Article

Not peer-reviewed version

Spatiotemporal Variability of Global Atmospheric Methane Observed from Two Decades of Satellite Hyperspectral Infrared Sounders

[Lihang Zhou](#) , [Juying Warner](#) ^{*} , [Nicholas R.Nalli](#) , Zigang Wei , [Youmi Oh](#) , Lori Bruhwiler , Xingpin Liu , [Murty Divakarla](#) , [Ken Pryor](#) , [Satya Kalluri](#) , [Mitch D. Goldberg](#)

Posted Date: 11 May 2023

doi: 10.20944/preprints202305.0782.v1

Keywords: Hyperspectral IR Sounding; Methane; CH4 Concentration; AIRS; CrIS; CH4 Trends



Preprints.org is a free multidiscipline platform providing preprint service that is dedicated to making early versions of research outputs permanently available and citable. Preprints posted at Preprints.org appear in Web of Science, Crossref, Google Scholar, Scilit, Europe PMC.

Copyright: This is an open access article distributed under the Creative Commons Attribution License which permits unrestricted use, distribution, and reproduction in any medium, provided the original work is properly cited.

Article

Spatiotemporal Variability of Global Atmospheric Methane Observed from Two Decades of Satellite Hyperspectral Infrared Sounders

Lihang Zhou ¹, Juying Warner ^{2,*}, Nicholas R. Nalli ^{3,4}, Zigang Wei ³, Youmi Oh ⁵, Lori Bruhwiler ⁵, Xingpin Liu ³, Murty Divakarla ^{3,4}, Ken Pryor ⁴, Satya Kalluri ¹ and Mitchell D. Goldberg ⁶

¹ NOAA JPSS Program Office, Lanham, MD 20706, USA

² Dept. of Atmospheric & Oceanic Science, University of Maryland, College Park, MD 20742

³ IM Systems Group, Inc., 3206 Tower Oaks, Blvd., Suite 300, Rockville, MD 20852, USA

⁴ NOAA/NESDIS Center for Satellite Applications and Research (STAR), 5830 University Research Court, MD 20740, USA

⁵ NOAA Global Monitoring Laboratory (GML), 325 Broadway R/GML, Boulder CO 80305-3328

⁶ NOAA NESDIS, 1335 East West Highway, Silver Spring, Maryland, 20910

* Correspondence: juying@atmos.umd.edu

Abstract: Methane (CH₄) is the second most significant contributor to climate change after carbon dioxide (CO₂), accounting for approximately 20% of the contributions from all the well-mixed greenhouse gases. Understanding the spatiotemporal distributions, and the relevant long-term trends are crucial to identifying the sources, sinks, and impacts on climate. Hyperspectral thermal infrared (TIR) sounders, including the Atmospheric Infrared Sounder (AIRS), the Cross-track Infrared Sounder (CrIS), and the Infrared Atmospheric Sounding Interferometer (IASI), have been used to measure global CH₄ concentrations since 2002. This study analyzed nearly twenty years of data from AIRS and CrIS and confirmed a significant increase in CH₄ concentrations in the mid-upper troposphere (around 400 hPa) from 2003 to 2020, with a total increase of approximately 85 ppb, representing a +4.8% increase in 18 years. The rate of increase was derived using global satellite TIR measurements is consistent with in-situ measurements, indicating a steady increase starting in 2007 and became stronger in 2014. The study also compared CH₄ concentrations derived from the AIRS and CrIS against ground-based measurements from NOAA Global Monitoring Laboratory (GML) and found phase shifts in the seasonal cycles in the middle to high latitudes in the northern hemisphere, which is attributed to the influence of stratospheric CH₄ that varies at different latitudes. These findings provide insights into the global budget of atmospheric composition and the understanding of satellite measurement sensitivity of CH₄.

Keywords: hyperspectral IR sounding; CH₄ concentration; CH₄ seasonality; satellite CH₄ trends; AIRS; CrIS

1. Introduction

Atmospheric methane (CH₄) is the second most critical greenhouse gas and responsible for ≈20% of the direct lower-tropospheric warming caused by well-mixed greenhouse gases [1–3]. According to climate data records reconstructed from polar ice cores [4,5], the concentration of CH₄ in 2019 has more than doubled since pre-industrial times [6] (IPCC AR6 2021, A.2.1). CH₄ has a much shorter atmospheric lifetime (about one decade) than CO₂ (longer than one century), while each CH₄ molecule has a global warming potential of 84 and 28 times greater than CO₂ for time spans of 20 and 100 years, respectively [3,6–8]. CH₄ may have caused as much as half of the global temperature increase since preindustrial times [6]. It is therefore critical to monitor the global distribution of, and changes in, CH₄ and gain understanding of the response and impact on the climate and environment [9–16].

Since current ground-based measurements are sparse, especially in remote land-based source regions, measurements from environmental satellites play an important role to assess CH₄ concentrations by providing continuous spatiotemporal observations [17]. In the last two decades, a

series of satellite passive sensors have been launched by international space agencies to provide observations of atmospheric CH₄ as well as other greenhouse gas (GHG) concentrations. Among these observing systems have been the Scanning Imaging Absorption spectrometer for Atmospheric Chartography (SCIAMACHY) onboard the European Space Agency (ESA) ENVISAT (2003–2012), which operated in the UV, visible, and near-infrared (near-IR) spectral regions [18], followed by the Thermal and Near-infrared Sensor for carbon Observation (TANSO) onboard the Japanese JAXA/NIES/MOE Greenhouse gases Observing Satellite (GOSAT), which has been in operation since 2009, along with GOSAT-2 starting in 2018 [19–21]. These NIR sensors were recently joined by the Tropospheric Monitoring Instrument (TROPOMI) onboard the Copernicus Sentinel-5 Precursor (S5P) satellite, launched in October 2017 [22], along with GHGSat, launched in June 2016 [23]. The CH₄ products derived from these NIR sensors measure a total column average from hyperspectral measurements of reflected NIR radiation scattered and absorbed by CH₄ with the spectra range from 1.6 to 2.3 μm , which include a mixture of surface and column atmospheric source contributions. The applications of the NIR sensors have demonstrated capabilities of mapping the regional distribution and detecting point source anomalies. Other source imagers soon to be launched, such as MethaneSAT, GeoCarb, and Carbon Mapper, etc., can also detect emissions from individual facilities [24].

In addition to these passive sensors, and of specific interest to this work, are the hyperspectral thermal infrared (TIR) sounders onboard the polar orbiting satellites, the Atmospheric Infrared Sounder (AIRS) onboard the NASA Earth Observing System (EOS)/Aqua [25], the Cross-track Infrared Sounder (CrIS) onboard the Suomi National Polar orbiting Partnership (SNPP) and NOAA-20 [26], as well as the Infrared Atmospheric Sounding Interferometer (IASI) operating on Metop satellites provided by Centre National d'Etudes Spatiales (CNES, France) [27], have also been used to derive CH₄ concentration. These hyperspectral sounders were originally designed for retrievals of the atmospheric temperature and moisture soundings, and the channels near 7.66 μm absorption band can be used to detect the mid-tropospheric column methane concentration. Over the past two decades, global CH₄ environmental data records (EDRs) have been continuously generated by exploiting data from these hyperspectral TIR sensors. The currently operating and planned future hyperspectral TIR sounders are listed in Table 1 [7].

Several previous studies have been conducted to demonstrate uses of the hyperspectral TIR measurements for evaluation of the free tropospheric methane concentration, for example Xiong et al. [28] for AIRS, and Razavi [29] for IASI, and Smith and Barnet [30] for CrIS. In this paper, we analyze the spatiotemporal global distributions, and long-term trends, especially the latitudinal and seasonality dependencies of the CH₄ concentration derived from the advanced hyperspectral sounders flown in the same 01:30/13:30 local equator crossing time (LEXT) orbits (i.e., CrIS and AIRS). To gain insight into the changes between the surface and upper tropospheric CH₄, the satellite retrievals from AIRS and CrIS are also compared with NOAA Global Monitoring Laboratory (GML) in-situ observations and model outputs. The AIRS physical retrieval algorithm has been adapted at NOAA for application to the operational CrIS system (with ongoing updates and improvements). This has enabled the provision of consistent atmospheric vertical profile EDRs from 2002 to the present. The CrIS sensor is a part of the technical baseline for the JPSS program satellites, so these hyperspectral TIR data and profile EDRs are expected to extend through the JPSS-4 timeframe into the 2040s.

Section 2 described the data sources and retrieval methodology. The global CH₄ distributions, the rate of changes, and the latitudinal variations derived from the satellite data are presented in Section 3. The results are discussed in Section 4, followed by conclusions in Section 5.

Table 1. Hyperspectral TIR Sounders onboard LEO Environmental Satellites.

Satellite	Instruments (Providing Agency)	LEXT	Launch dates
-----------	-----------------------------------	------	--------------

Aqua	AIRS (NASA)	01:30/13:30	2002
Metop-A,-B,-C	IASI (CNES)	09:30/21:30	2006, 2012, 2018
SNPP, JPSS-1,2,3,4	CrIS (NASA)	01:30/13:30	2011, 2017, 2022, 2027, 2032
Metop-SG-A1,2,3	IASI-NG (CNES)	09:30/21:30	2024, 2031, 2037

2. Methods

2.1. CrIS and AIRS Observations

The CrIS instruments are Fourier transform spectrometers and their characteristics and channel information are described by previous studies [31–36]. We use data spanning back to December 2014, when the SNPP CrIS instrument was operating in full spectral resolution at 0.625 cm^{-1} in all 3 bands, and a total of 2211 channels [32]. AIRS is an IR grating spectrometer with 2378 discrete channels as described by studies [25,37,38]. AIRS has demonstrated an estimated stability of $\sim 4\text{ mK/year}$ [39]. The radiometric stability of the AIRS radiances has been recently estimated to be better than 0.02 to 0.03 K per decade versus the minor-gas anomalies to the NOAA/GML in situ measurements in several AIRS channels, which are within the levels of climate trending which are roughly on the order of 0.1 K per decade [40].

2.2. The AIRS and CrIS Retrieved CH_4 Profiles

The AIRS science team retrieval algorithm is described in Susskind et al. (2003) [41], including the sensor calibration, microwave (MW) first guess retrieval, cloud-clearing, initial first guess IR retrieval, and a final IR physical retrieval. The cloud-clearing step enables the use of partially cloudy measurements [42,43]. Validation and improvements of AIRS retrievals are described in Fetzer et al. [44], Tobin et al. [45], Divakarla et al. [46], Chahine et al. [38], Susskind et al. [47], Nalli et al. [48], and many other studies. Because of the AMSU-A2 instrument failure, AIRS products using both TIR and MW were discontinued after 24 September 2016. Thus, for a consistent data record, we use AIRS Version 7 IR-only retrievals for the entire record from the NASA Goddard Earth Sciences (GES) Data and Information Services Center (DISC) (<https://disc.gsfc.nasa.gov>) [49].

The NOAA Unique Combined Atmospheric Processing System (NUCAPS) is the NOAA operational retrieval algorithm for the operational hyperspectral thermal IR sounders [50]. The NUCAPS algorithm is based on the AIRS science team retrieval algorithm Version 5 [30,41,47] which differs primarily in the first guess methodology (v5 uses a linear Eigenvector regression, whereas v7 uses a neural network nonlinear regression) [41]. The NUCAPS algorithm runs operationally at NOAA/NESDIS, with the operational products being publicly available from the Comprehensive Large Array-data Stewardship System (CLASS).

Both the AIRS and NUCAPS CrIS retrieval algorithms use spectral channels near $7.66\text{ }\mu\text{m}$ to retrieve CH_4 [28,29]. The CH_4 channel selection is based on the sensitivity to CH_4 as indicated by the kernel functions [51,52]. To reduce interference from other absorbing species, channels with overlapping absorption bands (e.g., water vapor and HNO_3), are minimized. The AIRS and NUCAPS CH_4 retrievals are in general sensitive in the range between 650 hPa and the lower stratosphere, with peak sensitivity around 300-400 hPa, depending on surface and atmospheric conditions [53]. The CH_4 weighting function, or Jacobian matrix, describes the portion of the CH_4 profile represented by each radiance measurement [53]. An example of the CrIS CH_4 Jacobian matrix, calculated from the Standalone AIRS Radiative Transfer Algorithm (SARTA, see algorithm description in Strow et al., 2003), is shown in Figure 1. From Figure 1, it is clear that the most CH_4 -sensitive region is the middle to upper troposphere (i.e., $\sim 200 - 600\text{ hPa}$), as depicted in the non-red color shades in Figure 1. The peak of the sensitivity can be higher or lower depending on the local scenario of CH_4 profiles.

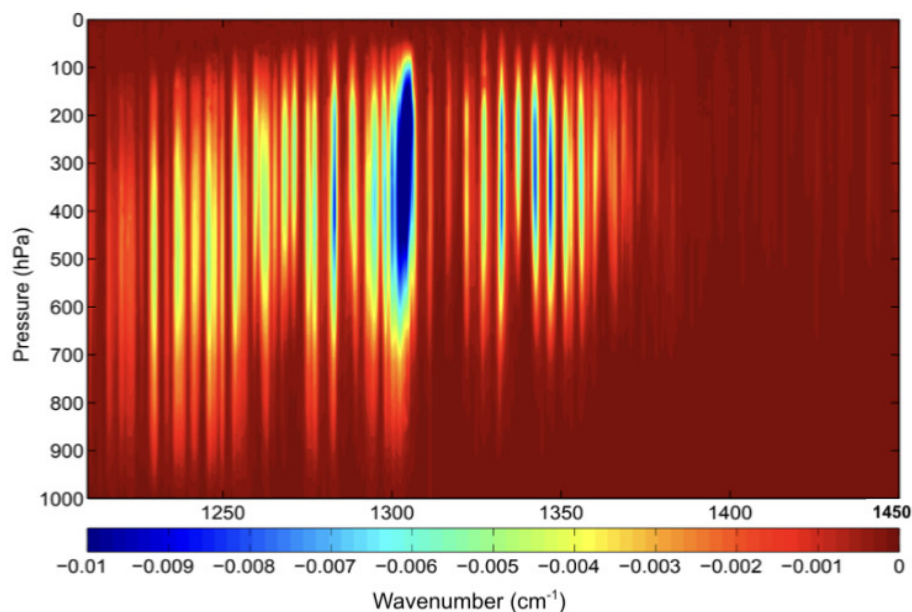


Figure 1. CH₄ Jacobians for CrIS based on an example atmospheric profile for 15°N latitude: the x- and y-axes show spectral wavenumbers (cm⁻¹) and the vertical pressure coordinate (hPa), respectively.

Prior to the CH₄ retrieval step in the algorithm, the atmospheric vertical temperature and moisture profiles (AVTP and AVMP, respectively), surface skin temperatures, and land emissivity are retrieved using different channels than those used for CH₄ retrievals. This data, as well as the a priori profiles of CH₄, are used as inputs to SARTA forward calculation [56]. The difference between the observed and calculated radiances (obs minus calc) is minimized to construct an error covariance matrix, from which the change of CH₄ is derived using an eigenvector transformation and damping. The final retrieved profile of CH₄ is usually obtained through several iterations. For more details on the NUCAPS and AIRS algorithm, see Susskind et al. [41,58], the NUCAPS Algorithm Theoretical Basis Document (ATBD) (2021), and Smith and Barnett [30]; for the details of the CH₄ first guess and channel selections, see Warner et al. [51], and Xiong et al. [28], and Gambacorta et al. [52].

The NUCAPS CH₄ retrieval has been significantly improved over the last 2 years. The major changes include updates of the CH₄ and N₂O a priori, quality control criteria, and refinements in the CH₄ channel selection. There were also other NUCAPS algorithm improvements, such as the updated TIR spectral tuning (i.e., an empirical radiance bias correction), which improved the performance of the NUCAPS temperature and water vapor retrievals, which in turn had a positive impact on the downstream CH₄ products. The CH₄ retrievals from CrIS on SNPP and NOAA-20 have gone through a thorough validation process by comparison to in-situ data and similar products from other satellite sensors [59–61]. For the AIRS and CrIS CH₄ products, we estimated a precision of 1%. While the same retrieval approach was used for AIRS and NUCAPS algorithms, the differences in the sensors, channels, a priori, tuning, and quality control, can contribute to the differences in CH₄ retrievals between AIRS and CrIS.

2.3. CH₄ Ground Observation Network

NOAA GML has been recording CH₄ measurements since 1983 at a globally distributed network of in situ surface sampling sites [62]. The network was originally designed to sample the global “background” atmosphere far from strong local sources, and despite some increase in coverage over time, the network remains sparse in space and time. More recently, in situ profiles have been added using a network of light aircraft, communications towers, and balloon-borne samplers. These measurements are well characterized and provide invaluable information for global CH₄ monitoring [63]. GML profile observations from aircraft, balloon-borne, and AirCore have been used as the truth

for the validation of the NUCAPS CH₄ profile retrievals [61]. In this study, we use the long-term GML in situ measurements in our analysis of TIR satellite CH₄ for comparison purposes. Because most GML data are collected at the surface or in the lower troposphere, while TIR retrievals are mostly sensitive to the middle to upper troposphere, direct comparisons are not possible. Nevertheless, the interannual differences between the in situ and TIR satellite observations provide valuable insights into vertical contrasts due to transport.

3. Results

3.1. CH₄ Global Distributions

The CH₄ time series from nearly two decades (2003 - 2020) of AIRS v7 retrievals [12,58,64,65] were analyzed in this study. As described in previous section 2.2, the AIRS methane retrievals are broadly sensitive in the range between 850 hPa and the lower stratosphere, with peak sensitivity around 300-400 hPa, depending on surface and atmospheric conditions. Figure 2 displays annual mean global maps of satellite retrieved CH₄ at 400 hPa for 2003 (left panel) and 2020 (right panel). The maps show similar patterns of the global CH₄ distribution, such as higher concentrations over the northern hemisphere (NH), the large-scale transport of plumes from biomass burning over Africa and South America, and large industrial emissions over Asia. Global CH₄ concentrations significantly increased over this time period, with the annual average in 2003 at ~1754 parts per billion (ppb), and ~1839 ppb in 2020. The total increase during this period was approximately 85 ppb which represents a ~4.8% increase. For the same time period (2003-2020), the annual average of CH₄ concentrations observed from the GML surface measurements is ~1777 ppb in 2003, and ~1879 ppb in 2020 which is roughly a 5.7% increase. The satellite CH₄ concentrations from TIR sounders, which represent a broad layer roughly spanning 200-400 hPa [62], are lower than the GML in situ measurements, as expected, due to the latter's proximity to the source regions. Note that while the recent versions of AIRS algorithm (V7, and V6) have implemented improvements of methane retrievals over previous versions (V5 and earlier), there might still be artifacts in the retrievals due to uncertainties in surface emissivity (especially over land/snow/ice surfaces) and cloud contamination in the cloud-cleared radiances that affect Figure 2. There are ongoing efforts to improve the AIRS retrieval algorithms [66].

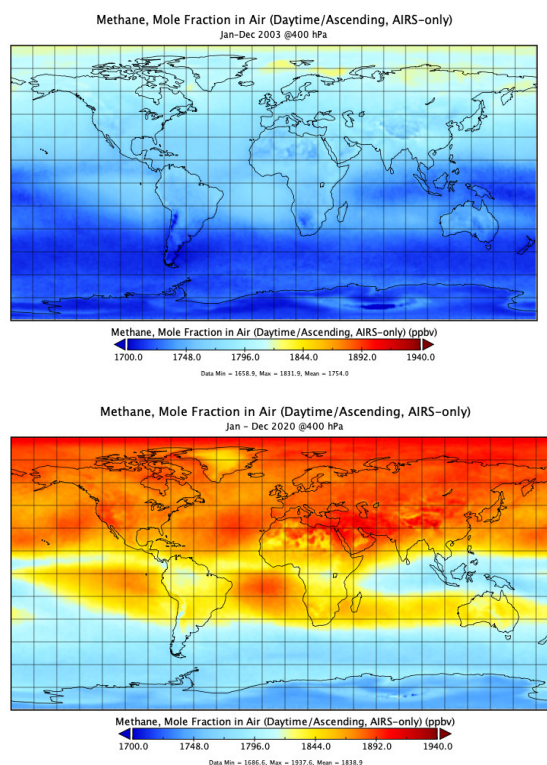


Figure 2. Annual mean of AIRS retrieved atmospheric CH₄ spanning a broad layer with an effective pressure of ≈400 hPa for the years 2003 (left) and 2020 (right), using the same color scale (Data processed and downloaded from NASA GES Giovanni, and plotted with Panoply).

3.2. Rate of Change of CH₄ Concentrations from Satellite TIR Measurements

The global mean growth rate of CH₄ co has been changing over the last three decades [63] (Dlugokencky et al. 2003). The global growth rate of CH₄ based on GML in situ measurements was 11.9 ± 0.9 ppb yr⁻¹ from 1984 to 1989, declined from 1990 to 1998, and then reached nearly zero growth from 1999 to 2005 [13,67,68]. A renewed strong growth in global CH₄ began in 2006 [10,14,68]. Growth in global CH₄ has been accelerating recently, further increasing from 2015 to 2020 [9]. The annual CH₄ concentration increases in 2020 was 15.19 ± 0.41 ppb yr⁻¹ (https://gml.noaa.gov/ccgg/trends_CH4/), which was the largest annual increase recorded since 1983, when NOAA/GML's ongoing measurements began [70].

We attempt to examine the same trends using global TIR satellite measurements spanning the last decades. We follow the fitting methods of Nisbet et al. (2016) [71] as below:

We fit a monthly averaged CH₄ time series at each latitude with a 2nd order polynomial and 4 harmonic frequencies,

$$y(t) = y_p(t) + y_s(t) + E(t) \quad (1)$$

Where $y_p(t)$ represents trend signal,

$$y_p(t) = p_0 + p_1t + p_2t^2 \quad (2)$$

And $y_s(t)$ represents seasonal signals,

$$y_s(t) = \sum_{k=1}^4 [A_k \sin(2\pi kt) + B_k \cos(2\pi kt)] \quad (3)$$

$k=1, 2, 3, 4$ represents the 1-year, 1/2-year, 1/3-year and 1/4-year periods. $E(t)$ represents the fitting residuals, which is filtered by a low pass filter, i.e., at roughly 2 years,

$$E(t) = E_{low}(t) + \varepsilon \quad (4)$$

Where $E_{low}(t)$ denotes the signal passed by the low band filter, and ε is the high frequency noise. y_p is paired with $E_{low}(t)$ to form the long-term trend of CH₄ monthly mean, that is

$$y_n(t) = y_p(t) + E_{low}(t) \quad (5)$$

Then the annual CH₄ growth rate for each month may be calculated as

$$R(t) = \frac{dy_n(t)}{dt} = \frac{dy_p(t) + dE_{low}(t)}{dt} \quad (6)$$

The evolution of CH₄ zonal distributions are shown in the upper panels of Figure 3 where the top left panel shows AIRS measurements, and the top right panel are the same measurements but with fitting, as described above. Whereas globally the CH₄ concentrations increased for all latitudes over time, stronger increases were observed in the NH in the earlier years, and beginning around 2008, the increases gradually expanded to the Southern Hemisphere (SH) and the arctic region. The lower panels of Figure 3 show the rate of change calculated from the AIRS and CrIS TIR observations where the bottom left and right are the de-seasoned growth rates of AIRS and CrIS, respectively. The rate of change from AIRS also demonstrated the overall increase of CH₄ after 2008, especially the increases that have been expanding toward the SH and polar region. The results from CrIS for 2015 to 2020 show general agreement with those from AIRS for the same period. Since it takes approximately one year for CH₄ to be mixed from the surface throughout the troposphere, the years with strong regional growth are usually followed by declines to the global background [72]. This pattern can be clearly seen from the early 2000s, but after 2014 the period of decline became less well-defined and more dominant as seen by the overall positive increase rates. The satellite TIR results presented here are also generally consistent with those derived from in situ measurements [73].

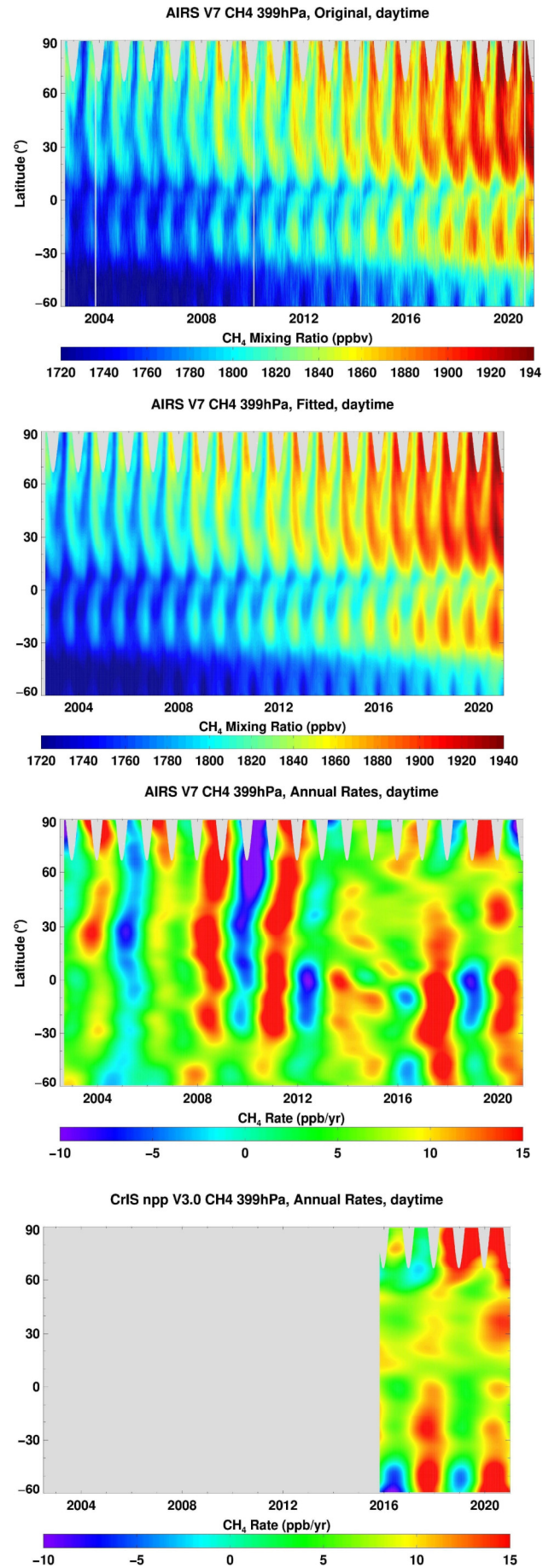


Figure 3. CH₄ zonal distributions with time (upper panel); AIRS raw (upper left); and AIRS fitted (upper right); and the corresponding rate of change from AIRS (lower left), and CrIS (lower right).

3.3. Inter-Polar CH₄ Difference

The zonal changes in CH₄ concentrations have been discussed in previous studies [9,70]. CH₄ concentrations are generally higher in the NH than the SH due to emission sources predominantly from NH land surfaces. The black curve in Figure 4 shows the averaged zonal mean variations from a 19-year average of AIRS CH₄ data at 400 hPa (2003-2021). The lowest value (~1730 ppb, leftmost) is over the Antarctic region, and the highest value (~1858 ppb, rightmost) is over the Arctic region. The absolute CH₄ Inter-Polar Difference (IPD: the difference between zonal averages calculated for 60-90°N and 60-90°S) for the period is ~128 ppb. The zonal means from each year from 2003 to 2021 are also shown in Figure 4. The increase in the south pole region is the smallest, compared with increases in the other latitudes. The two largest peaks of the increases in Figure 4 are in the north and south sup-tropical zones.

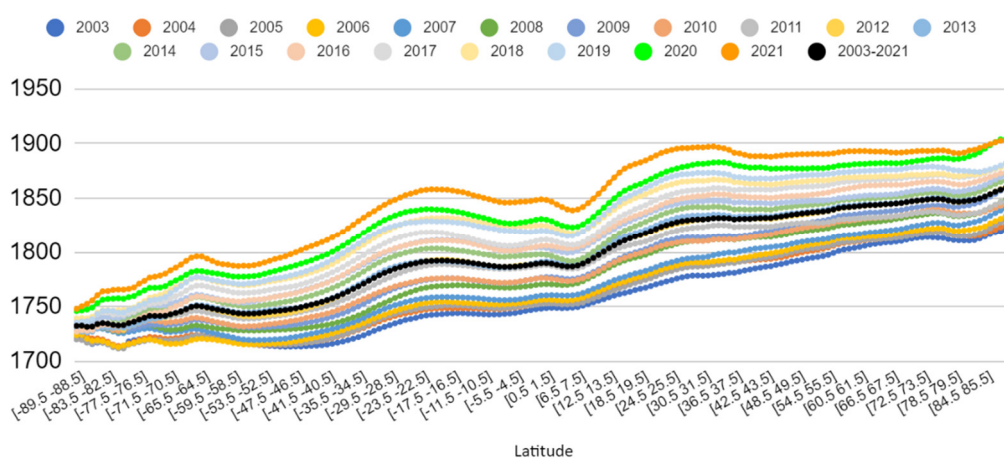


Figure 4. Zonal means of AIRS v7 tropospheric CH₄ near 400 hPa (in ppb) vertical level for each year from 2003 to 2021, and the black line represents the averaged 19 years of AIRS data from 2003 to 2021.

3.4. Latitudinal Variations

To understand the latitudinal variation of TIR-derived CH₄, we examined the time series of CH₄ over different latitudinal zones retrieved from AIRS and CrIS, and compared those with the GML in situ measurements. It is here important to keep in mind that the TIR-based measurements represent a broad tropospheric layer roughly spanning 200-400 hPa. Figure 5 shows the CH₄ time series (centered at 400 hPa) for latitude ranges of 60 – 90°N (top panel), 30 – 60°N (2nd panel), 0 – 30°N (3rd panel), 30°S – 0 (4th panel), and 60 – 30°S (lowest panel) respectively. The CH₄ retrievals from AIRS (blue lines, 2003 - 2020) and CrIS (orange lines, 2015 - 2020) agree well with each other, both showing that the overall tropospheric CH₄ concentrations have been increasing across all latitudinal zones. The trends are similar to those of the GML in situ observations (green lines, 2003 - 2020), although the magnitudes of the CH₄ concentrations derived from each measurement approach can vary.

The CH₄ concentrations show annual cycles that vary at different latitudes. As seen in Figure 5, the amplitudes of the annual cycle are higher for the mid-and high- latitudes in the NH than they are in the tropics, this primarily because of the CH₄ sources being mostly located in the NH mid-to-high-latitudes. Additionally, microbial sources (especially wetlands) can have a strong seasonality, and more importantly, chemistry controls the seasonal cycles. In fact, at the surface in the NH, the minimum occurs in summer when the microbial sources could be expected to be the strongest. Also, seasonal differences in transport play a role. Figure 5 shows clearly that the TIR retrieved CH₄ from AIRS and CrIS have an overall negative bias than those from GML in the NH, which is consistent with CH₄ concentrations being higher in the boundary layer from source regions at the surface and decreases in the free troposphere.

The in situ CH_4 measurements from GML are larger than AIRS CH_4 by 105 ppb at $60 - 90^\circ\text{N}$, 122 ppb at $30 - 60^\circ\text{N}$, and 56 ppb at $0 - 30^\circ\text{N}$, respectively. However, in the SH, the CH_4 retrievals at 400 hPa are higher than or close to those from the surface observations. On average, the AIRS CH_4 is 4 ppb higher than those from GML in the SH, and 0.5 ppb for CrIS.

Figure 5 also shows a prominent phase shift in the annual cycles of satellite TIR retrievals and the in situ measurements, especially in the mid-to-high NH latitudes. This phase shift is not obvious in the low latitudes in both the NH and SH. In arctic region (60 to 90°N), the tropospheric CH_4 concentrations retrieved from AIRS and CrIS show about 7–8 months of lag to the in-situ concentrations. Similar phase shifts are observed in the NH mid-latitudes ($30-60^\circ\text{N}$), with lags of about 4-5 months. Such lags are minimal for the NH and SH tropics (30°S to 30°N).

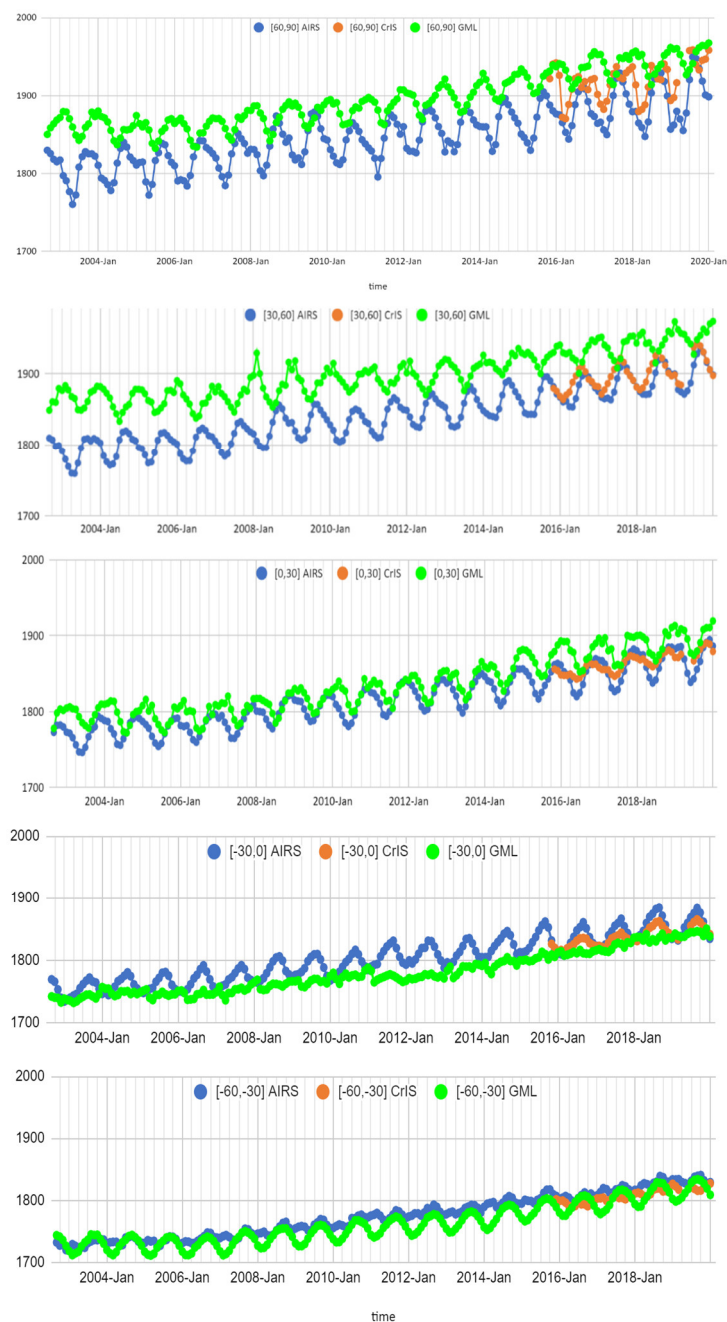


Figure 5. Time series of CH_4 (in ppb) retrieved from AIRS (blue), CrIS (orange) at 400 hPa, and in situ measurements from NOAA GML (green) for different latitudinal zones: $60-90^\circ\text{N}$ (top panel); $30-60^\circ\text{N}$ (2nd panel); $0-30^\circ\text{N}$ (3rd panel); $0-30^\circ\text{S}$ (4th panel); $30-60^\circ\text{S}$ (lowest panel).

The AIRS CH₄ in SH mid-latitudes showed two peaks in the seasonal cycles, one of which represents the same seasonal cycle as in GML in situ measurements, whereas the other peak shows similar phase shift as in the NH mid-latitude. The SH high latitudes are not shown due to noisy retrievals contaminated by the Southern Ocean clouds.

4. Discussion

To understand better the vertical phase shifts in CH₄ seasonality, we examined the results from CarbonTracker-CH₄ [74,75]. CarbonTracker-CH₄ is NOAA GML's global atmospheric inversion system to estimate emissions of atmospheric CH₄ by assimilating global in-situ measurements [76]. Since the first version of CarbonTracker-CH₄ was published in 2014, we revised our inversion system by jointly assimilating measurements of CH₄ and the stable isotopic ratio of CH₄ (denoted $\delta^{13}\text{C-CH}_4$), incorporating spatially- and temporally- resolved source signature of $\delta^{13}\text{C-CH}_4$, and optimizing fluxes at a grid-scale. The current CarbonTracker-CH₄ is based on the TM5-4DVAR inversion system [77] and simulates optimized monthly global microbial, fossil, and pyrogenic emissions at $3 \times 2^\circ$ horizontal resolution (longitude by latitude) from 1997 to 2021. Based on the optimized emissions, the mole fraction of atmospheric CH₄ is simulated at 3-hourly, $3 \times 2^\circ$ horizontal resolution with 25 vertical hybrid sigma pressure levels. Since CarbonTracker-CH₄ assimilates CH₄ mole fraction from more than 330 in-situ sites, the simulated CH₄ mole fractions of the surface layer match well with the surface in-situ measurements.

The CH₄ time series for different vertical levels and latitudinal bands from the CarbonTracker-CH₄ model runs are shown in Figure 6. Seven pressure levels are plotted from 200 to 800 hPa at 100-hPa intervals for every 30° latitudinal band. Similar phase shifts to those seen by the satellite TIR measurements described in Section 3.3, can also be seen in these model results. The seasonality of CarbonTracker-CH₄ results at 800 hPa (Dark blue in Figure 6) resembles the seasonality of GML in-situ measurements (Green in Figure 5), and the seasonality of CarbonTracker-CH₄ at 300-400 hPa (Green and sky blue in Figure 6) resembles AIRS/CrIS seasonality at 400 hPa (Blue and Orange in Figure 5). The seasonality of CarbonTracker-CH₄ at 200 hPa shows the influence of stratospheric chemistry (Figure 7). The seasonality of CarbonTracker-CH₄ at 300-400 hPa is influenced by both tropospheric (500-800 hPa) and stratospheric chemistry (200 hPa). The magnitude of the vertical shifts in CH₄ seasonality likely depends on the age and transport processes of CH₄ for the different zonal bands.

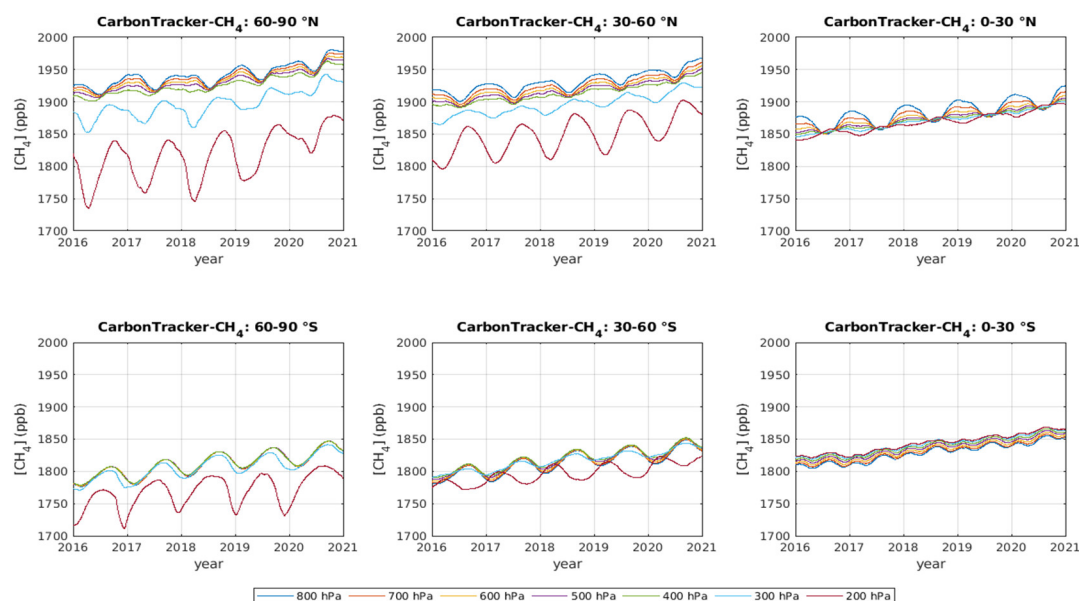


Figure 6. Time series of zonally averaged CH₄ from GML CarbonTracker-CH₄ from 2003 to 2020 at 200-800 hPa for different zonal bands: 60-90°N (upper left); 30-60°N (upper middle); 0-30°N (upper right); 90-60°S (lower left); 60-30°S (lower middle); and 30°S-0 (lower right).

The tropics (30°S to 30°N) show smaller vertical gradients than temperate and polar latitudinal bands, due to strong convection from Hadley cells (Webster 2004). There are minimal phase shifts between the stratosphere and troposphere compared to the mid-to-high NH latitudes. For latitudes 0-30°N, CarbonTracker-CH₄ at 300-400 hPa did not show a large seasonality (Top-right plot in Figure 6), consistent with CrIS results. For latitude 0-30°S, there are two peaks throughout vertical layers, a larger peak in summer and a smaller peak in winter, consistent with GML's in-situ measurements at Tutuila, American Samoa (Bottom-right plot in Figure 6).

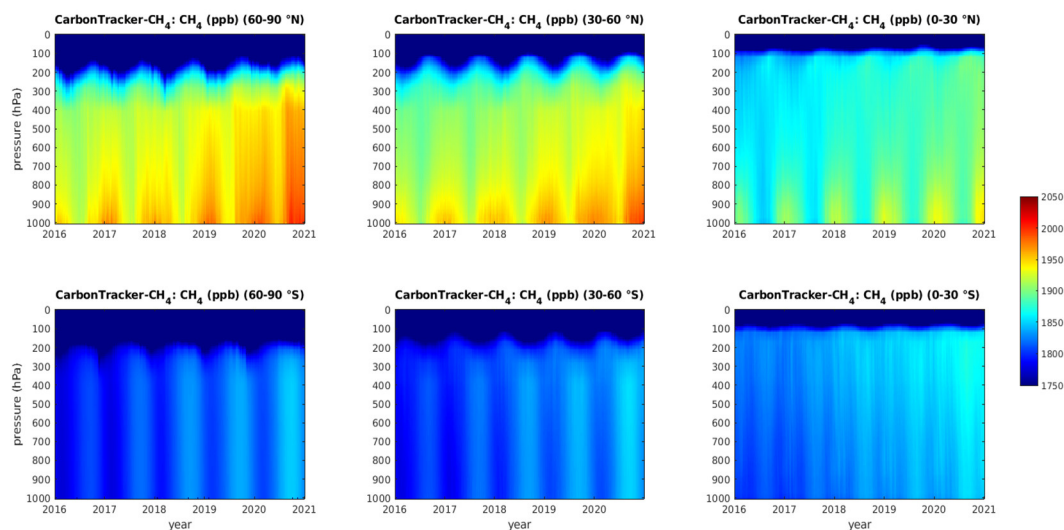


Figure 7. Pressure-altitude versus time cross-sections of CH₄ from CarbonTracker-CH₄ from 2003 to 2020 for different zonal bands: 60-90°N (upper left); 30-60°N (upper middle); 0-30°N (upper right); 90-60°S (lower left); 60-30°S (lower middle); and 30°S-0 (lower right).

Figure 7 shows curtain plots of vertical cross sections of CH₄ over time, for the different global polar, midlatitude, and tropical bands as discussed previously. Similar phase shifts are observed for the NH latitudes, and strong vertical gradients occur in the tropopause regions for NH midlatitude and polar zones. In the SH, CH₄ concentrations remain almost constant throughout the troposphere. This may be attributed to the lack of emission sources in the SH. From Figs. 6 and 7, the results show that for the broad layer between 200 hPa and 400 hPa, where the TIR (AIRS and CrIS) retrievals are most sensitive, the retrievals may be influenced by stratospheric CH₄. The magnitude of the stratospheric influence varies with different latitude zones, depending on factors such as tropopause heights and deep convection. Specifically, in the NH mid- and high-latitude regions, stratospheric CH₄ seems to dominate the seasonality of retrieval results, whereas the SH mid-latitudes information is the mix of tropospheric and stratospheric CH₄ information.

5. Conclusions

Hyperspectral thermal IR (TIR) sounders, such as AIRS and CrIS (as well as IASI), provide continuous long-term global data records of the mid-to-upper tropospheric CH₄. In this study, we analyzed spatial and temporal variation using AIRS and CrIS remote sensing measurements. Significant changes have been found for CH₄ concentrations at annual and inter-annual time scales, and at various latitudes. Increases in CH₄ concentrations and annual growth rates have also been studied. Our analyses showed strong increasing trends in the mid-to-upper troposphere from satellite measurements. There are latitudinal dependences of these increases, as well as seasonal dependencies.

We compared the TIR-retrieved broad-layer CH₄ concentrations with the GML global in situ observation network and discovered temporal phase shifts of the CH₄ seasonality between the two data sources. The phase shifts are most significant in the NH, where the surface emissions are higher. We conclude that the CH₄ broad-layer concentrations from satellite TIR measurements are influenced

by stratospheric contributions that represent different seasonality from the troposphere in the NH mid- to high- latitudes. This phase shift behavior is minimal in the low latitudes in both NH and SH, and in the SH mid-latitudes the retrieved CH₄ information is influenced by both troposphere and stratosphere. Additional analysis is needed to fully understand the seasonal phase differences between the surface and upper tropospheric/lower stratospheric, which may include more in-depth model studies and high-altitude flight observations. Longer-term annual to interannual trend studies are also important to comprehend global changes in CH₄ distributions. The CrIS sensors from NOAA-21 (launched successfully in November 2022), along with the planned future low earth orbit (LEO) satellite missions will help to serve this goal.

Acknowledgments: This publication describes the collective work of government industry and academic teams over the course of many years. The authors would like to thank especially the following JPSS STAR NUCAPS and NOAA GML teams for their contributions: Banghua Yan, Alisa Young, Tom Atkins, Changyong Cao, Flavio Iturbide-Sanchez, Tong Zhu, Changyi Tan, Tianyuan Wang, Antonia Gambacorta, Chris Barnett, Walter Wolf, Thomas S. King, Mike Wilson, Ninghai Sun, Priyanka Roy, Colm Sweeney, Diane Stanitski, Helen Wood, Arlyn Andrews, Andy Jacobson, Bianca Baier, Jim Butler, Xin Lan, and other colleagues. The manuscript contents are solely the opinions of the authors and do not constitute a statement of policy, decision, or position on behalf of NOAA or the U.S. government. The authors also wish to acknowledge the availability of the in situ measurements provided by NOAA Global Monitoring Laboratory (GML), the AIRS version 7 level 2 CH₄ products from NASA Earthdata center (Data citation: AIRS project (2019), Aqua/AIRS L3 Monthly Standard Physical Retrieval (AIRS-only) 1 degree x 1 degree V7.0, Greenbelt, MD, USA, Goddard Earth Sciences Data and Information Services Center (GES DISC), Accessed 2 April 2022, 10.5067/UBENJB9D3T2H).

References

1. Ramanathan, V.; Cicerone, R.J.; Singh, H.B.; Kiehl, J.T. Trace Gas Trends and Their Potential Role in Climate Change. *J. Geophys. Res. Atmos.* **1985**, *90*, 5547–5566.
2. IPCC. Climate change: The scientific basis. In: Houghton JT, Ding Y, Griggs DJ, Noguer M, van der Linden PJ, Dai X, Maskell K, Johnson CA, editors. Contribution of working group I to the third assessment report of the intergovernmental panel on climate change. Cambridge: Cambridge University Press; 2001. p. 881. "<Wgi_Tar_Full_Report.Pdf>".
3. IPCC. Climate Change 2013: The Physical Science Basis. Contribution of Working Group I to the Fifth Assessment Report of the Intergovernmental Panel on Climate Change. [Stocker, T. F., D. Qin, G.-K. Plattner, M. Tignor, S. K. Allen, J. Boschung, A. Nauels, Y. Xia, V. Bex and P. M. Midgley (eds.)]. Cambridge University Press, Cambridge, United Kingdom and New York, NY, USA, 1585.
4. Etheridge, D.M.; Steele, L.P.; Francey, R.J.; Langenfelds, R.L. Atmospheric methane between 1000 A.D. and present: Evidence of anthropogenic emissions and climatic variability. *J. Geophys. Res. Atmos.* *103*, 15979–15993.
5. Rubino, M., D. M. Etheridge, D. P. Thornton, R. Howden, C. E. Allison, R. J. Francey, R. L. Langenfelds, L. P. Steele, C. M. Trudinger, D. A. Spencer, M. A. J. Curran, T. D. van Ommen, and A. M. Smith. "Revised Records of Atmospheric Trace Gases CO₂, CH₄, N₂O, and Δ13C-CO₂ over the Last 2000 years from Law Dome, Antarctica. *Earth Syst. Sci. Data* *11*, 473-92.
6. IPCC 2021: Climate Change 2021: The Physical Science Basis. Contribution of Working Group I to the Sixth Assessment Report of the Intergovernmental Panel on Climate Change [Masson-Delmotte, V., P. Zhai, A. Pirani, S.L. Connors, C. Péan, S. Berger, N. Caud, Y. Chen, L. Goldfarb, M.I. Gomis, M. Huang, K. Leitzell, E. Lonnoy, J.B.R. Matthews, T.K. Maycock, T. Waterfield, O. Yelekçi, R. Yu, and B. Zhou (eds.)]. Cambridge University Press. In the Press.
7. Crisp, D., Meijer, Y., Munro, R., Bowman, K. and Chatterjee, A. *A Constellation Architecture for Monitoring Carbon Dioxide and Methane from Space*. 2018.
8. Voulgarakis, A.; Naik, V.; Lamarque, J.-F.; Shindell, D.T.; Young, P.J.; Prather, M.J.; Wild, O.; Field, R.D.; Bergmann, D.; Cameron-Smith, P.; et al. Analysis of present day and future OH and methane lifetime in the ACCMIP simulations. *Atmospheric Meas. Tech.* *13*, 2563–2587.
9. Nisbet, E.G.; Manning, M.R.; Dlugokencky, E.J.; Fisher, R.E.; Lowry, D.; Michel, S.E.; Myhre, C.L.; Platt, S.M.; Allen, G.; Bousquet, P.; et al. Very Strong Atmospheric Methane Growth in the 4 Years 2014–2017: Implications for the Paris Agreement. *Glob. Biogeochem. Cycles* *33*, 318–342.

10. Nisbet, E. G., R. E. Fisher, D. Lowry, J. L. France, G. Allen, S. Bakkaloglu, T. J. Broderick, M. Cain, M. Coleman, J. Fernandez, G. Forster, P. T. Griffiths, C. P. Iverach, B. F. J. Kelly, M. R. Manning, P. B. R. Nisbet-Jones, J. A. Pyle, A. Townsend-Small, A. al-Shalaan, N. Warwick, and G. Zazzeri. Methane Mitigation: Methods to Reduce Emissions, on the Path to the Paris Agreement. *Rev. Geophys.* 58, e2019RG000675.
11. Fung, I.; John, J.; Lerner, J.; Matthews, E.; Prather, M.; Steele, L.P.; Fraser, P.J. Three-dimensional model synthesis of the global methane cycle. *J. Geophys. Res.* **1991**, 96, 13033–13065.
12. Worden, J.; Kulawik, S.; Frankenberg, C.; Payne, V.; Bowman, K.; Cady-Peirara, K.; Wecht, K.; Lee, J.-E.; Noone, D. Profiles of CH₄, HDO, H₂O, and N₂O with improved lower tropospheric vertical resolution from Aura TES radiances. *Atmospheric Meas. Tech.* 5, 397–411.
13. Dlugokencky, E.J.; Bruhwiler, L.; White, J.W.C.; Emmons, L.K.; Novelli, P.C.; Montzka, S.A.; Masarie, K.A.; Lang, P.M.; Crotwell, A.M.; Miller, J.B.; et al. Observational constraints on recent increases in the atmospheric CH₄ burden. *Geophys. Res. Lett.* 36.
14. Nisbet, E. G., E. J. Dlugokencky, and P. Bousquet. Atmospheric Science. Methane on the Rise--Again. *Science* 343, 493-5.
15. Saunio, M., A. R. Stavert, B. Poulter, P. Bousquet, J. G. Canadell, R. B. Jackson, P. A. Raymond, E. J. Dlugokencky, S. Houweling, P. K. Patra, P. Ciais, V. K. Arora, D. Bastviken, P. Bergamaschi, D. R. Blake, G. Brailsford, L. Bruhwiler, K. M. Carlson, M. Carrol, S. Castaldi, N. Chandra, C. Crevoisier, P. M. Crill, K. Covey, C. L. Curry, G. Etiope, C. Frankenberg, N. Gedney, M. I. Hegglin, L. Höglund-Isaksson, G. Hugelius, M. Ishizawa, A. Ito, G. Janssens-Maenhout, K. M. Jensen, F. Joos, T. Kleinen, P. B. Krummel, R. L. Langenfelds, G. G. Laruelle, L. Liu, T. Machida, S. Maksyutov, K. C. McDonald, J. McNorton, P. A. Miller, J. R. Melton, I. Morino, J. Müller, F. Murguía-Flores, V. Naik, Y. Niwa, S. Noce, S. O'Doherty, R. J. Parker, C. Peng, S. Peng, G. P. Peters, C. Prigent, R. Prinn, M. Ramonet, P. Regnier, W. J. Riley, J. A. Rosentreter, A. Segers, I. J. Simpson, H. Shi, S. J. Smith, L. P. Steele, B. F. Thornton, H. Tian, Y. Tohjima, F. N. Tubiello, A. Tsuruta, N. Viovy, A. Voulgarakis, T. S. Weber, M. van Weele, G. R. van der Werf, R. F. Weiss, D. Worthy, D. Wunch, Y. Yin, Y. Yoshida, W. Zhang, Z. Zhang, Y. Zhao, B. Zheng, Q. Zhu, Q. Zhu, and Q. Zhuang. "The Global Methane Budget 2000–2017. *Earth Syst. Sci. Data* 12, 1561-623.
16. Kirschke, Stefanie, Philippe Bousquet, Philippe Ciais, Marielle Saunio, Josep G. Canadell, Edward J. Dlugokencky, Peter Bergamaschi, Daniel Bergmann, Donald R. Blake, Lori Bruhwiler, Philip Cameron-Smith, Simona Castaldi, Frédéric Chevallier, Liang Feng, Annemarie Fraser, Martin Heimann, Elke L. Hodson, Sander Houweling, Béatrice Josse, Paul J. Fraser, Paul B. Krummel, Jean-François Lamarque, Ray L. Langenfelds, Corinne Le Quéré, Vaishali Naik, Simon O'Doherty, Paul I. Palmer, Isabelle Pison, David Plummer, Benjamin Poulter, Ronald G. Prinn, Matt Rigby, Bruno Ringeval, Monia Santini, Martina Schmidt, Drew T. Shindell, Isobel J. Simpson, Renato Spahni, L. Paul Steele, Sarah A. Strode, Kengo Sudo, Sophie Szopa, Guido R. van der Werf, Apostolos Voulgarakis, Michiel van Weele, Ray F. Weiss, Jason E. Williams, and Guang Zeng. "Three Decades of Global Methane Sources and Sinks. *Nat. Geosci.* 6, 813-23.
17. Jacob, D. J., A. J. Turner, J. D. Maasackers, J. Sheng, K. Sun, X. Liu, K. Chance, I. Aben, J. McKeever, and C. Frankenberg. "Satellite Observations of Atmospheric Methane and Their Value for Quantifying Methane Emissions. *Atmos. Chem. Phys.* 16, 14371-96.
18. Frankenberg, C.; Aben, I.; Bergamaschi, P.; Dlugokencky, E.J.; van Hees, R.; Houweling, S.; van der Meer, P.; Snel, R.; Tol, P. Global column-averaged methane mixing ratios from 2003 to 2009 as derived from SCIAMACHY: Trends and variability. *J. Geophys. Res. Atmos.* 116.
19. Yokota, T.; Yoshida, Y.; Eguchi, N.; Ota, Y.; Tanaka, T.; Watanabe, H.; Maksyutov, S. Global Concentrations of CO₂ and CH₄ Retrieved from GOSAT: First Preliminary Results. *SOLA*, 5, 160–163. <https://doi.org/10.2151/sola.2009-041>.
20. Schepers, D.; Guerlet, S.; Butz, A.; Landgraf, J.; Frankenberg, C.; Hasekamp, O.; Blavier, J.; Deutscher, N.M.; Griffith, D.W.T.; Hase, F.; et al. Methane retrievals from Greenhouse Gases Observing Satellite (GOSAT) shortwave infrared measurements: Performance comparison of proxy and physics retrieval algorithms. *J. Geophys. Res. Atmos.* 117.
21. Saitoh, N.; Touno, M.; Hayashida, S.; Imasu, R.; Shiomi, K.; Yokota, T.; Yoshida, Y.; Machida, T.; Matsueda, H.; Sawa, Y. Comparisons between XCH₄ from GOSAT Shortwave and Thermal Infrared Spectra and Aircraft CH₄ Measurements over Guam. *SOLA* 8, 145–149.
22. Lorente, A.; Borsdorff, T.; Butz, A.; Hasekamp, O.; de Brugh, J.A.; Schneider, A.; Wu, L.; Hase, F.; Kivi, R.; Wunch, D.; et al. Methane retrieved from TROPOMI: improvement of the data product and validation of the first 2 years of measurements. *Atmospheric Meas. Tech.* 14, 665–684.

23. Varon, D.J.; McKeever, J.; Jarvis, D.; Maasackers, J.D.; Pandey, S.; Houweling, S.; Aben, I.; Scarpelli, T.; Jacob, D.J. Satellite Discovery of Anomalous Large Methane Point Sources from Oil/Gas Production. *Geophys. Res. Lett.* **2019**, *46*, 13507–13516. <https://doi.org/10.1029/2019GL083798>.
24. Pandey, S.; Gautam, R.; Houweling, S.; van der Gon, H.D.; Sadavarte, P.; Borsdorff, T.; Hasekamp, O.; Landgraf, J.; Tol, P.; van Kempen, T.; et al. Satellite observations reveal extreme methane leakage from a natural gas well blowout. *Proc. Natl. Acad. Sci. USA* **2019**, *116*, 26376–26381. <https://doi.org/10.1073/pnas.1908712116>.
25. Aumann, H. H., M. T. Chahine, C. Gautier, M. D. Goldberg, E. Kalnay, L. M. McMillin, H. Revercomb, P.W. Rosenkranz, W. L. Smith, D. H. Staelin, L. L. Strow, and J. Susskind. AIRS/AMSU/HSB on the Aqua Mission: Design, Science Objectives, Data Products, and Processing Systems. *IEEE Trans. Geosci. Remote Sens.* *41*, 253–64.
26. Goldberg, M.D.; Kilcoyne, H.; Cikanek, H.; Mehta, A. Joint Polar Satellite System: The United States next generation civilian polar-orbiting environmental satellite system. *J. Geophys. Res. Atmos.* *118*, 13463–13475.
27. Hilton, F.; Armante, R.; August, T.; Barnet, C.; Bouchard, A.; Camy-Peyret, C.; Capelle, V.; Clarisse, L.; Clerbaux, C.; Coheur, P.-F.; et al. Hyperspectral Earth Observation from IASI: Five Years of Accomplishments. *Bull. Am. Meteorol. Soc.* *93*, 347–370.
28. Xiong, X.; Barnet, C.; Maddy, E.; Sweeney, C.; Liu, X.; Zhou, L.; Goldberg, M. Characterization and Validation of Methane Products from the Atmospheric Infrared Sounder (AIRS). *J. Geophys. Res.* **2008**, *113*.
29. Razavi, A.; Karagulian, F.; Clarisse, L.; Hurtmans, D.; Coheur, P.F.; Clerbaux, C.; Müller, J.F.; Stavrakou, T. Global distributions of methanol and formic acid retrieved for the first time from the IASI/MetOp thermal infrared sounder. *Atmospheric Meas. Tech.* *11*, 857–872. <https://doi.org/10.5194/acp-11-857-2011>.
30. Smith, N.; Barnet, C.D. Uncertainty Characterization and Propagation in the Community Long-Term Infrared Microwave Combined Atmospheric Product System (CLIMCAPS). *Remote. Sens.* *11*, 1227.
31. Lee, Thomas F., Craig S. Nelson, Patrick Dills, Lars Peter Riishojgaard, Andy Jones, Li Li, Steven Miller, Lawrence E. Flynn, Gary Jedlovec, William McCarty, Carl Hoffman, and Gary McWilliams. “NPOESS.” *Bull. Am. Meteorol. Soc.* *91*, 727–40.
32. Zou, Cheng-Zhi, Lihang Zhou, Lin Lin, Ninghai Sun, Yong Chen, Lawrence E. Flynn, Bin Zhang, Changyong Cao, Flavio Iturbide-Sanchez, Trevor Beck, Banghua Yan, Satya Kalluri, Yan Bai, Slawomir Blonski, Taeyoung Choi, Murty Divakarla, Yalong Gu, Xianjun Hao, Wei Li, Ding Liang, Jianguo Niu, Xi Shao, Larrabee Strow, David C. Tobin, Denis Tremblay, Sirish Uprety, Wenhui Wang, Hui Xu, Hu Yang, and Mitchell D. Goldberg. The Reprocessed Suomi SNPP Satellite Observations. *Remote Sens.* *12*, 2891.
33. Han, Yong, Henry Revercomb, Mike Crompt, Degui Gu, David Johnson, Daniel Mooney, Deron Scott, Larrabee Strow, Gail Bingham, Lori Borg, Yong Chen, Daniel DeSlover, Mark Esplin, Denise Hagan, Xin Jin, Robert Knuteson, Howard Motteler, Joe Predina, Lawrence Suwinski, Joe Taylor, David Tobin, Denis Tremblay, Chunming Wang, Lihong Wang, Likun Wang, and Vladimir Zavyalov. “Suomi Npp Cris Measurements, Sensor Data Record Algorithm, Calibration and Validation Activities, and Record Data Quality.” *J. Geophys. Res. Atmos.* *118*, 12,734–12,48.
34. Han, Y.; Chen, Y. Calibration Algorithm for Cross-Track Infrared Sounder Full Spectral Resolution Measurements. *IEEE Trans. Geosci. Remote. Sens.* *56*, 1008–1016.
35. Sanchez, F, Tobin, D.Strow, Scott D. Mooney D. Johnson D. Suwinski L. Predina J, Bolen D. Guenther B. Yan B. Noaa-20 Cris Sdr Report for Validated Maturity Review. NOAA JPSS Science Review. 2018. Available online: https://www.star.nesdis.noaa.gov/jpss/documents/AMM/N20/Cris_SDR_Validated.pdf (accessed on 17 March 2021).
36. Yan, B.; Goldberg, M.; Jin, X.; Liang, D.; Huang, J.; Porter, W.; Sun, N.; Zhou, L.; Pan, C.; Iturbide-Sanchez, F.; et al. A New 32-Day Average-Difference Method for Calculating Inter-Sensor Calibration Radiometric Biases between SNPP and NOAA-20 Instruments within ICVS Framework. *Remote. Sens.* *13*, 3079.
37. Pagano, T.; Aumann, H.; Hagan, D.; Overoye, K. Pre-launch and in-flight radiometric calibration of the atmospheric infrared sounder (AIRS). *IEEE Trans. Geosci. Remote. Sens.* *41*, 265–273.
38. Chahine, Moustafa T., Thomas S. Pagano, Hartmut H. Aumann, Robert Atlas, Christopher Barnet, John Blaisdell, Luke Chen, Murty Divakarla, Eric J. Fetzer, Mitch Goldberg, Catherine Gautier, Stephanie Granger, Scott Hannon, Fredrick W. Irion, Ramesh Kakar, Eugenia Kalnay, Bjorn H. Lambriksen, Sung-Yung Lee, John Le Marshall, W. Wallace McMillan, Larry McMillin, Edward T. Olsen, Henry Revercomb, Philip Rosenkranz, William L. Smith, David Staelin, L. Larrabee Strow, Joel Susskind, David Tobin, Walter Wolf, and Lihang Zhou. *AIRS. Bull. Am. Meteorol. Soc.* *87*, 911–926.

39. Aumann, Hartmut H. and Thomas S. Pagano. Using AIRS and IASI data to evaluate absolute radiometric accuracy and stability for climate applications. Proc. SPIE 7085, Atmospheric and Environmental Remote Sensing Data Processing and Utilization IV: Readiness for Geos II, 2008, 708504. <https://doi.org/10.1117/12.795225>.
40. Strow, L.L.; DeSouza-Machado, S. Establishment of AIRS climate-level radiometric stability using radiance anomaly retrievals of minor gases and sea surface temperature. *Atmospheric Meas. Tech.* **13**, 4619–4644.
41. Susskind, J.; Barnet, C.D.; Blaisdell, J.M. Retrieval of atmospheric and surface parameters from AIRS/AMSU/HSB data in the presence of clouds. *IEEE Trans. Geosci. Remote Sens.* **41**, 390–409.
42. Smith, W.L. An improved method for calculating tropospheric temperature and moisture from satellite radiometer measurements. *Mon. Weather Rev.* **1968**, *96*, 387–396.
43. Chahine, M.T. Remote Sounding of Cloudy Atmospheres. I. The Single Cloud Layer. *J. Atmospheric Sci.* **1974**, *31*, 233–243.
44. Fetzer, E., L. M. McMillin, D. Tobin, H. H. Aumann, M. R. Gunson, W. W. McMillan, D. E. Hagan, M. D. Hofstadter, J. Yoe, D. N. Whiteman, J. E. Barnes, R. Bennartz, H. Vomel, V. Walden, M. Newchurch, P. J. Minnett, R. Atlas, F. Schmidlin, E. T. Olsen, M. D. Goldberg, Zhou Sisong, Ding HanJung, W. L. Smith, and H. Revercomb. AIRS/AMSU/HSB Validation. *IEEE Trans. Geosci. Remote Sens.* **41**, 418–431.
45. Tobin, D.C.; Revercomb, H.E.; Knuteson, R.O.; Lesht, B.M.; Strow, L.L.; Hannon, S.E.; Feltz, W.F.; Moy, L.A.; Fetzer, E.J.; Cress, T.S. Atmospheric Radiation Measurement Site Atmospheric State Best Estimates for Atmospheric Infrared Sounder Temperature and Water Vapor Retrieval Validation. *J. Geophys. Res.* **111**.
46. Divakarla, M.G.; Barnet, C.D.; Goldberg, M.D.; McMillin, L.M.; Maddy, E.; Wolf, W.; Zhou, L.; Liu, X. Validation of Atmospheric Infrared Sounder Temperature and Water Vapor Retrievals with Matched Radiosonde Measurements and Forecasts. *J. Geophys. Res.* **111**.
47. Susskind, J.; Blaisdell, J.M.; Iredell, L.; Keita, F. Improved Temperature Sounding and Quality Control Methodology Using AIRS/AMSU Data: The AIRS Science Team Version 5 Retrieval Algorithm. *IEEE Trans. Geosci. Remote Sens.* **49**, 883–907.
48. Nalli, N.R.; Clemente-Colón, P.; Minnett, P.J.; Szczodrak, M.; Morris, V.; Joseph, E.; Goldberg, M.D.; Barnet, C.D.; Wolf, W.W.; Jessup, A.; et al. Ship-based measurements for infrared sensor validation during Aerosol and Ocean Science Expedition. *J. Geophys. Res.* **2004**, *111*, D09S04. <https://doi.org/10.1029/2005JD006385>.
49. Yue, Q and B. Lambrigtsen. Airs Version 7 Level 2 Performance Test and Validation Report (2020). Jet Propulsion Laboratory, California Institute of Technology.
50. Kalluri, S.; Barnet, C.; Divakarla, M.; Esmaili, R.; Nalli, N.; Pryor, K.; Reale, T.; Smith, N.; Tan, C.; Wang, T.; et al. Validation and Utility of Satellite Retrievals of Atmospheric Profiles in Detecting and Monitoring Significant Weather Events. *Bull. Am. Meteorol. Soc.* **103**, E570–E59.
51. Warner, X. Juying; et al., Operational Trace Gas Products Algorithms and Quality Evaluation in NOAA Unique CrIS/ATMS Processing Systems, in preparation (2022).
52. Gambacorta, Antonia, and Chris Barnet. Methodology and Information Content of the NOAA NESDIS Operational Channel Selection for the Cross-Track Infrared Sounder (CrIS). *Geosci. Remote Sens. IEEE Trans.* **51**, 3207–3216.
53. Gambacorta, A.; Barnet, C.; Wolf, W.; King, T.; Maddy, E.; Strow, L.; Xiong, X.; Nalli, N.; Goldberg, M. An Experiment Using High Spectral Resolution CrIS Measurements for Atmospheric Trace Gases: Carbon Monoxide Retrieval Impact Study. *IEEE Geosci. Remote Sens. Lett.* **11**, 1639–1643.
54. Rodgers, C.D. Retrieval of atmospheric temperature and composition from remote measurements of thermal radiation. *Rev. Geophys.* **1976**, *14*, 609–624.
55. Rodgers, C. Characterization and Error Analysis of Profiles Retrieved from Remote Sounding Measurements. *J. Geophys. Res.* **1990**, *95*, 5587–5595.
56. Conrath, B.J. Vertical Resolution of Temperature Profiles Obtained from Remote Radiation Measurements. *J. Atmospheric Sci.* **29**, 1262–1271.
57. Maddy, E.S.; Barnet, C.D. Vertical Resolution Estimates in Version 5 of AIRS Operational Retrievals. *IEEE Trans. Geosci. Remote Sens.* **46**, 2375–2384.
58. Strow, L. L., S. E. Hannon, S. De Souza-Machado, H. E. Motteler, and D. Tobin. An Overview of the AIRS Radiative Transfer Model. *IEEE Trans. Geosci. Remote Sens.* **41**, 303–313.
59. Susskind, J.; Blaisdell, J.M.; Iredell, L. Improved methodology for surface and atmospheric soundings, error estimates, and quality control procedures: the atmospheric infrared sounder science team version-6 retrieval algorithm. *J. Appl. Remote Sens.* **8**, 084994.

60. Zhou, L.; Divakarla, M.; Liu, X. An Overview of the Joint Polar Satellite System (JPSS) Science Data Product Calibration and Validation. *Remote. Sens.* **8**, 139.
61. Nalli, N.R.; Barnet, C.D.; Reale, A.; Tobin, D.; Gambacorta, A.; Maddy, E.S.; Joseph, E.; Sun, B.; Borg, L.; Mollner, A.K.; et al. Validation of satellite sounder environmental data records: Application to the Cross-track Infrared Microwave Sounder Suite. *J. Geophys. Res. Atmos.* **118**, 13,628–13,643.
62. Nalli, N.R.; et al. Validation of Carbon Trace Gas Profile Retrievals from the NOAA-Unique Combined Atmospheric Processing System for the Cross-Track Infrared Sounder. *Remote. Sens.* **12**, 3245.
63. Dlugokencky, E.J.; Steele, L.P.; Lang, P.M.; Masarie, K.A. The growth rate and distribution of atmospheric methane. *J. Geophys. Res.* **99**, 17021–17043.
64. WMO Gas Station report 2020 - WMO Global Atmosphere Watch (GAW) World Data Center for Greenhouse Gas (WDCGG) Data Summary No 43, March 2020. Available online: <https://gaw.kishou.go.jp/static/publications/summary/sum43/sum43.pdf>.
65. Kahn, B.H.; Irion, F.W.; Dang, V.T.; Manning, E.M.; Nasiri, S.L.; Naud, C.M.; Blaisdell, J.M.; Schreier, M.M.; Yue, Q.; Bowman, K.W.; et al. The Atmospheric Infrared Sounder version 6 cloud products. *Atmospheric Meas. Tech.* **14**, 399–426.
66. Thrastarson, H. Th., ed., 2021: AIRS/AMSU/HSB Version 7 Level 2 Product User Guide. Available online: https://docserver.gesdisc.eosdis.nasa.gov/public/project/AIRS/V7_L2_Product_User_Guide.pdf.
67. Ding, F.; Savtchenko, A.; Hearty, T.; Wei, J.; Theobald, M.; Vollmer, B.; Tian, B.; Fetzer, E. Assessing the Impacts of Two Averaging Methods on AIRS Level 3 Monthly Products and Multiyear Monthly Means. *J. Atmospheric Ocean. Technol.* **37**, 1027–1050.
68. Dlugokencky, E. J., S. Houweling, L. Bruhwiler, K. A. Masarie, P. M. Lang, J. B. Miller, and P. P. Tans. Atmospheric Methane Levels Off: Temporary Pause or a New Steady-State? *Geophys. Res. Lett.* **30**.
69. Steele, L.P.; Dlugokencky, E.J.; Lang, P.M.; Tans, P.P.; Martin, R.C.; Masarie, K.A. Slowing down of the global accumulation of atmospheric methane during the 1980s. *Nature* **358**, 313–316.
70. Chandra, N.; Patra, P.K.; Bisht, J.S.H.; Ito, A.; Umezawa, T.; Saigusa, N.; Morimoto, S.; Aoki, S.; Janssens-Maenhout, G.; Fujita, R.; et al. Emissions from the Oil and Gas Sectors, Coal Mining and Ruminant Farming Drive Methane Growth over the Past Three Decades. *J. Meteorol. Soc. Jpn. Ser. II* **2021**, *99*, 309–337, and <https://doi.org/10.2151/jmsj.2021-015>.
71. Nisbet, E.G.; Dlugokencky, E.J.; Manning, M.R.; Lowry, D.; Fisher, R.E.; France, J.L.; Michel, S.E.; Miller, J.B.; White, J.W.C.; Vaughn, B.; et al. Rising atmospheric methane: 2007–2014 growth and isotopic shift. *Glob. Biogeochem. Cycles* **30**, 1356–1370.
72. Butler J. H., Stephen A. Montzka NOAA Annual Greenhouse Gas Index (AGGI), 2021. Available online: <https://gml.noaa.gov/aggi/aggi.html>.
73. Lan, X.; Nisbet, E.G.; Dlugokencky, E.J.; Michel, S.E. What do we know about the global methane budget? Results from four decades of atmospheric CH₄ observations and the way forward. *Philos. Trans. R. Soc. A: Math. Phys. Eng. Sci.* **379**, 20200440.
74. Basu, S.; Lan, X.; Dlugokencky, E.; Michel, S.; Schwietzke, S.; Miller, J.B.; Bruhwiler, L.; Oh, Y.; Tans, P.P.; Apadula, F.; et al. Estimating emissions of methane consistent with atmospheric measurements of methane and $\delta^{13}\text{C}$ of methane. *Atmospheric Meas. Tech.* **2022**, *22*, 15351–15377.
75. Bruhwiler, L., Dlugokencky, E., Masarie, K., Ishizawa, M., Andrews, A., Miller, J., Sweeney, C., Tans, P., & Worthy, D. CarbonTracker-CH₄: An assimilation system for estimating emissions of atmospheric methane. *Atmos. Chem. Phys.* **2014**, *14*, 8269–8293.
76. Lan, X., Thoning, K. W., & Dlugokencky, E. J. (2023). Trends in globally-averaged CH₄, N₂O, and SF₆ determined from NOAA Global Monitoring Laboratory measurements. Version 2023-02. <https://doi.org/10.15138/P8XG-AA10>.
77. Bousserrez, N.; Henze, D.K.; Perkins, A.; Bowman, K.W.; Lee, M.; Liu, J.; Deng, F.; Jones, D.B.A. Improved analysis-error covariance matrix for high-dimensional variational inversions: application to source estimation using a 3D atmospheric transport model. *Q. J. R. Meteorol. Soc.* **2015**, *141*, 1906–1921.

Disclaimer/Publisher's Note: The statements, opinions and data contained in all publications are solely those of the individual author(s) and contributor(s) and not of MDPI and/or the editor(s). MDPI and/or the editor(s) disclaim responsibility for any injury to people or property resulting from any ideas, methods, instructions or products referred to in the content.